Journal of Manufacturing Processes 121 (2024) 20–34

Contents lists available at ScienceDirect

Journal of Manufacturing Processes

journal homepage: www.elsevier.com/locate/manpro

Full length article

High efficiency polishing of micro-structured NiP alloy using isotropic electrochemical etching for achieving sub-nanometer roughness

Jun Yang [a], Jingtian Ye [a], Guoxing Liu [a], Zixin Ye [a], Weijie Cui [a], Xinquan Zhang [a,*], Hui Deng [b,*]

[a] School of Mechanical Engineering, Shanghai Jiao Tong University, Shanghai 200240, China
[b] Department of Mechanical and Energy Engineering, Southern University of Science and Technology, 518055, China

ARTICLE INFO

Keywords:
Nickel phosphorus alloy
Sub-nanometer roughness
Shape-preserving polishing
Micro machining

ABSTRACT

Electroless plated nickel phosphorus (NiP) alloy is an essential engineered material used in optical applications, particularly in the field of extreme ultraviolet (EUV) technology, where high reflectivity of short-wavelength light is required. However, it is still challenging to achieve highly efficient sub-nanometer polishing of NiP plating, especially for micro-structured NiP surface. This study introduces isotropic etching polishing (IEP) as a novel ultra-precision processing technique for NiP plating, which is a damage-free and quick metal polishing technology through the amalgamation of contiguous etching pits. IEP was performed for 4 mins, leading to the attainment of a sub-nanometer surface exhibiting a Sa roughness of 0.065 nm, which verified efficiency and feasibility of the method. The IEP of NiP plating under various applied voltages is categorized into three stages: the etching stage, the limited current plateau stage, and the gas evolution stage. Experimental results bear witness to the direct correlation between the material removal rate (MRR) and surface roughness of NiP plating, specifically in relation to the sulfuric acid content within various electrolyte ratios. The most efficacious electrolyte composition was found to be 5:100 (H_2SO_4:CH_3OH). Furthermore, the technology achieved ultra-smooth and shape-preserving polishing with a surface roughness below 0.1 nm, as confirmed by the comparisons of both the grating microstructure and Fresnel lens before and after IEP. The findings presented in this study are highly valuable for comprehending the process development and viability of IEP for NiP plating.

1. Introduction

Metallic mirrors with outstanding optical, mechanical, and thermal properties find applications in various modern optical fields, including lithographic processors [28], astronomical observation projects [22], high power laser systems [4] and ultra-precision metrology systems [37]. In optical applications, aluminum, copper, and beryllium are extensively employed as materials for metal mirrors. [31]. Copper is frequently utilized in laser science applications owing to its superior thermal conductivity [33]. Simultaneously, aluminum exhibits desirable characteristics such as lightweight nature, facile formability, and exceptional reflectivity, particularly for shorter wavelengths [5]. However, beryllium is infrequently employed due to its toxic nature [31]. Aluminum mirrors can be readily finished by using Single Point Diamond Turning (SPDT), with a surface roughness below 3 nm [31]. Conversely, in ultra-short wavelength applications, such as extreme ultraviolet light, the metal mirror's surface roughness must be within the sub-nanometer range. This aspect becomes particularly crucial in the context of extreme ultraviolet lithography (EUV), which facilitates the production of electronic circuits at a significant scale with feature sizes of 22 nm and even smaller. In this regard, it is imperative to ensure a significant emission of power at the specific wavelength of 13.5 nm [20,27,29]. In a laser-produced plasma extreme ultraviolet lithography system, the collector mirror assumes the critical role of serving as the primary optical component. The collector mirror's role is to reflect and gather extreme ultraviolet light. In order to augment the reflectivity of 13.5 nm extreme ultraviolet (EUV) light, it is necessary for the surface of the collector mirror to exhibit a high-spatial frequency roughness (HSFR) below the threshold of 0.2 nm [8].

To fabricate an EUV collector mirror, an integration of ultra-precision manufacturing techniques and subsequent polishing steps has been employed. The process of Single-Point Diamond Turning (SPDT) is widely recognized for its ability to achieve high-precision surface quality and economical manufacturing of metallic mirrors. However, surfaces machined by SPDT exhibit periodic structures, leading to a surface roughness of approximately 5 nm [14]. For optimal performance in the EUV spectral range, it is essential to eliminate the typical diamond turning structure through polishing to completely

* Corresponding authors.

https://doi.org/10.1016/j.jmapro.2024.05.010
Received 23 August 2023; Received in revised form 4 March 2024; Accepted 1 May 2024
1526-6125/© 2024 Published by Elsevier Ltd on behalf of The Society of Manufacturing Engineers.

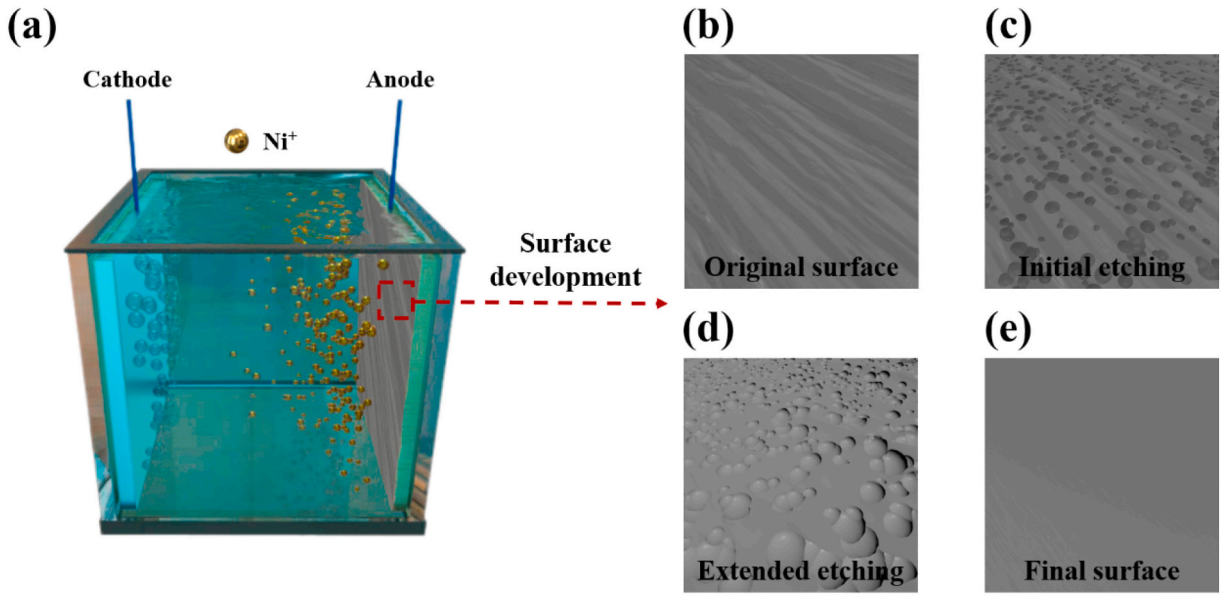

Fig. 1. Schematic depiction of the setup of experiment (a) and elucidation of the mechanism of IEP (b-e).

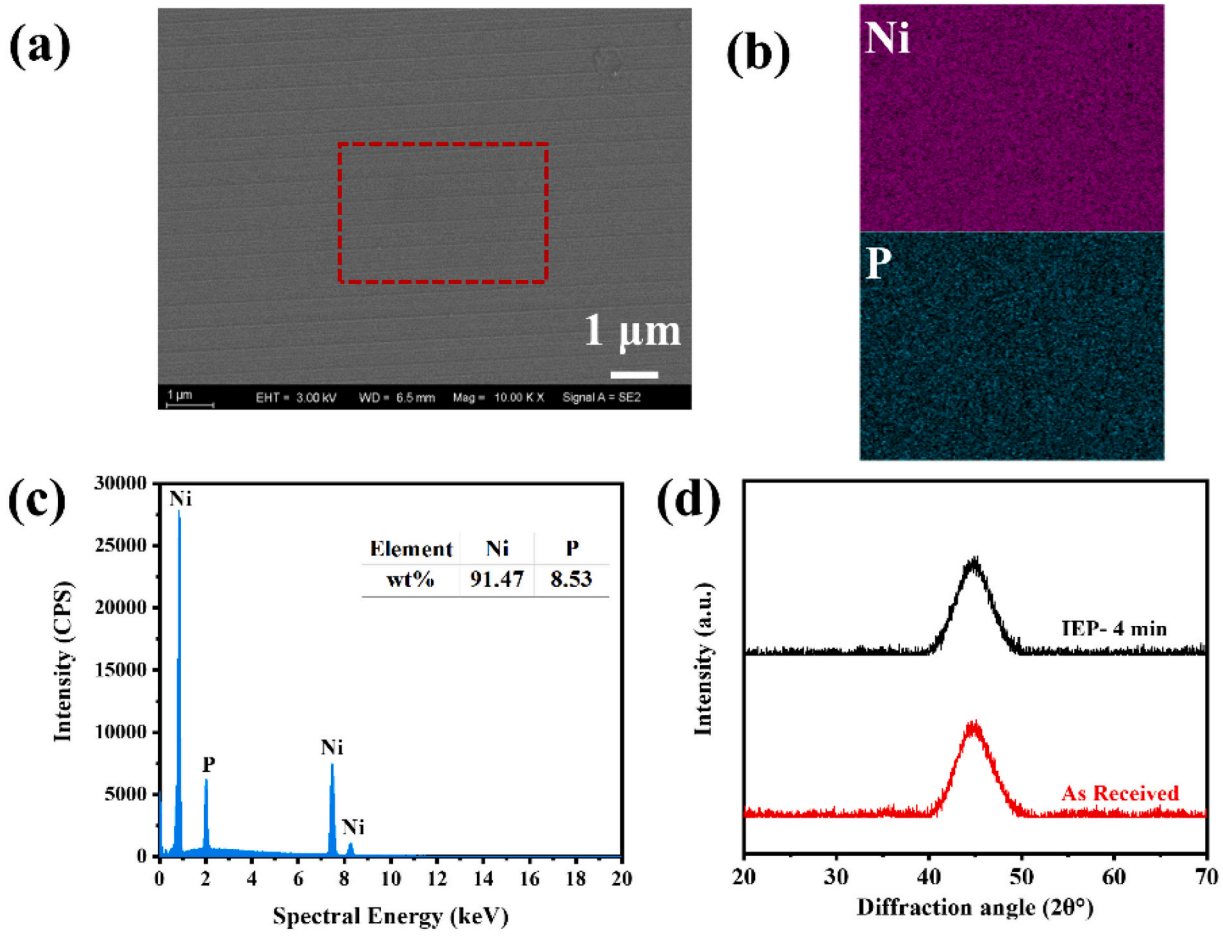

Fig. 2. The SEM image (a), EDS mapping (b), element content distribution (c) of As-received NiP plating. XRD profiles of NiP plating (d), as received and after IEP at 7 V voltage for 4 mins in 10 mL H_2SO_4 electrolyte.

decrease scatter losses. However, aluminum alone cannot be processed to attain the requisite level of surface roughness below 0.3 nm [34]. Moreover, the combination of an aluminum substrate with an amorphous nickel-phosphorous layer presents a viable solution for the manufacturing of super polished substrates [25]. Electroless nickel plating (NiP plating) offers a viable solution for two crucial aspects [24,26]. First, NiP plating is hard enough to be machined by SPDT. Second, NiP plating is an amorphous material, hence it has the higher

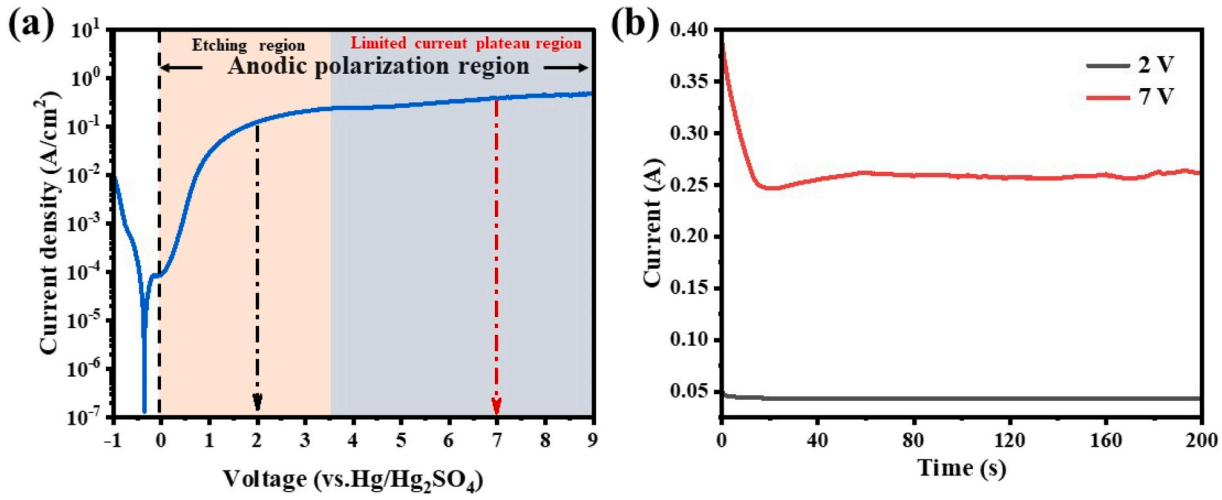

Fig. 3. (a) Polarized curve of NiP plating in an electrolyte with a volume ratio of H_2SO_4 to CH3OH of 10:100; (b) current-time plots obtained at different voltages.

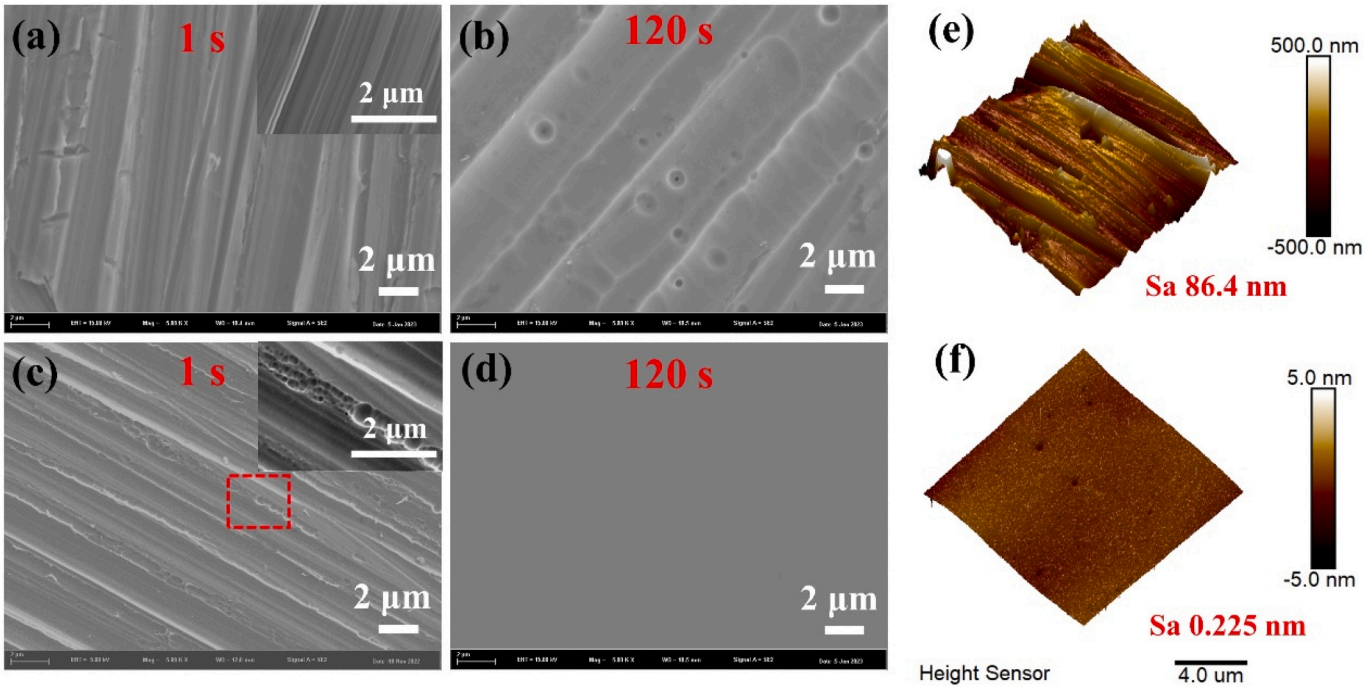

Fig. 4. Morphology and roughness of surface measured by SEM and AFM through varying states. (a) 1 s and (b, e) 120 s at the voltage of 2 V; (c) 1 s and (d, f) 120 s at the voltage of 7 V.

binding force with the base material. Consequently, the implementation of NiP plating on collector mirrors facilitates the enhancement of surface quality [33]. Research has demonstrated that a thick plating of a NiP alloy serves as a suitable polishing layer, enabling the achievement of a surface roughness below 1 nm [31].

The pursuit of ultra-precision polishing technology aspires to attain a surface roughness of nanometer or sub-nanometer magnitude through micro-abrasive or physical and chemical means. [3,21,41]. Its primary objective is to minimize residual surface irregularities and subsurface layers, eliminate defects from previous processes, and enhance surface roughness to obtain a smooth and low-stress surface. Various methods are employed for ultra-precision polishing, including magneto-rheological finishing (MRF) [19], small-tools Polishing (STP) [6], stressed-lap polishing (SLP) [17], airbag polishing [32], abrasive jet surface polishing (AJP) [35]. However, these methods involve direct contact with the workpiece during processing, leading to inevitable surface damage. Furthermore, due to limitations of the precision in the polishing tools themselves, achieving an ultra-smooth workpiece surface is unattainable.

In contrast, electrochemical polishing (ECP), commonly referred to as electropolishing, is a finishing technique employed to remove material of an alloy or metal through dissolution of anode [10,16]. The ECP is a contactless and non-destructive technology characterized by immersing the workpiece in a temperature-controlled electrolyte bath. The workpiece fulfills the role of the anode and establishes a connection with the positive electrode of a DC/AC power supply, while the negative electrode establishes the connection with the cathode. Through this arrangement, electric current flow from the anode, resulting in the selective dissolution of surface metal. Simultaneously, a reaction emerges at the cathode, typically resulting in the production of hydrogen. Over past few decades, ECP achieved wide-ranging applications in the final processing of multiple multi-metallic materials, including tungsten [36],

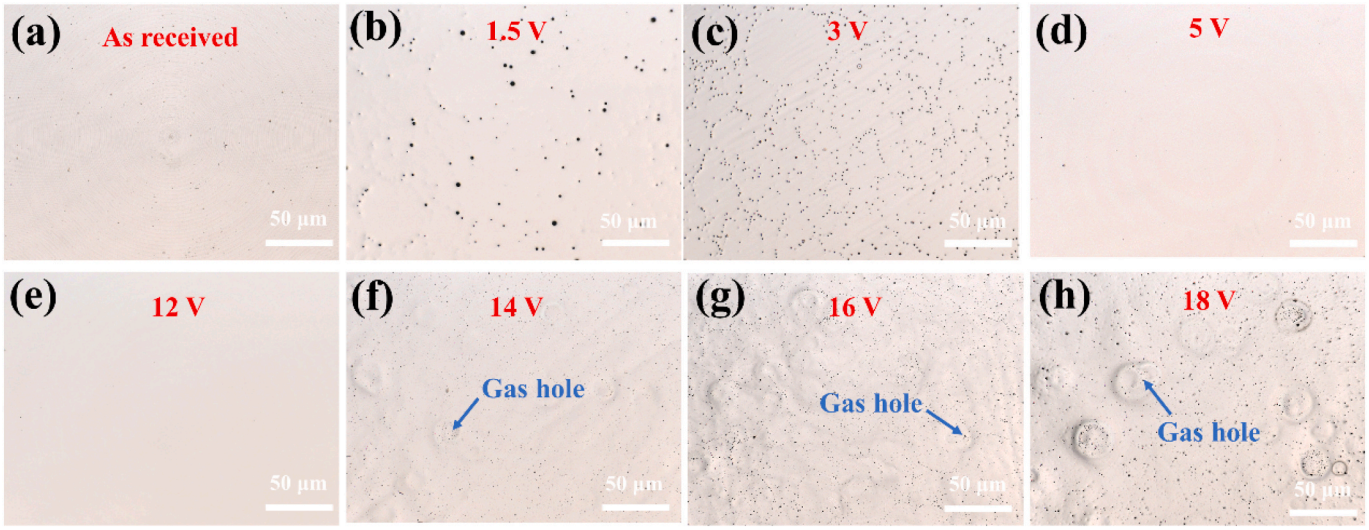

Fig. 5. Morphology of NiP plating by LSCM under different voltage: (a) As received; (b) 1.5 V; (c) 3 V; (d) 5 V; (e) 12 V; (f) 14 V; (g) 16 V and (h) 18 V for 240 s.

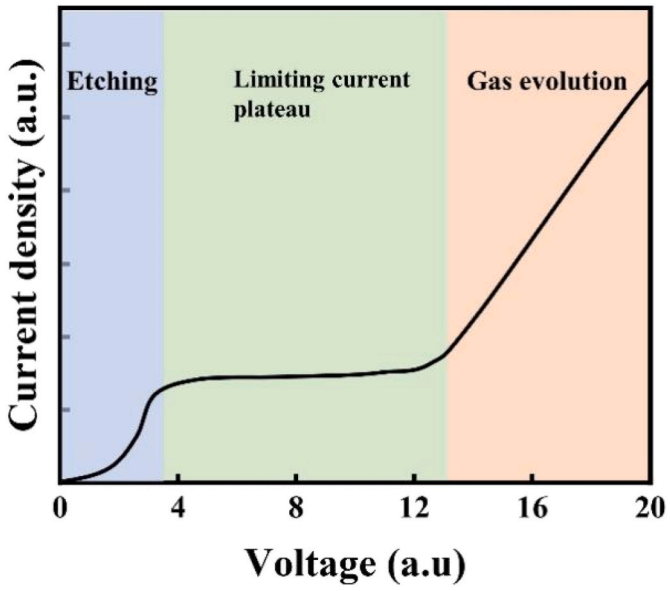

Fig. 6. The current density-voltage curve of electropolishing.

stainless steel [1], titanium [13], copper [15], aluminum [30]. Despite its extensive use, the precise mechanism underlying the ECP process remains incompletely understood [10]. Several theoretical models have been proposed to explain the polishing mechanism, with the passivation film model by Jacquet being the most widely accepted [38]. This film exhibits high viscosity and resistance. Importantly, its thickness is non-uniform, with the concave regions exhibiting greater thickness than the convex regions. Importantly, its thickness is non-uniform, with the concave regions exhibiting greater thickness than the convex regions. Consequently, the bulge dissolves at a relatively rapid rate, leading to a macroscopic polishing of the rough surface. However, the traditional electrochemical polishing technology has an electrolyte harmful to the environment, low material removal efficiency, and cannot achieve sub-nanometer roughness polishing effect. Therefore, it is necessary to improve the current electrochemical polishing technology and theoretical basis for the NiP plating.

In recent years, Yi et al. [39] introduced the comprehensive isotropic electrochemical polishing (IEP)method for alloys and metals, demonstrating its theoretical and experimental viability. This technique functions by disrupting the passivation layer through anode potential, causing the emergence of isotropic holes on the workpiece. Over time, these holes progressively enlarge and combine, ultimately yielding the polished substrate surface characterized by smoothness and luster. Inconel 718 [2], tungsten [40], aluminum alloy 6063 and pure nickel [39] were successfully polished by IEP with smooth surface and efficient processing speed. In addition to the electrochemical properties shared by both IEP and ECP processes, the IEP technique necessitates lower energy consumption because of the destruction of the passivation layer. Notably, the surface roughness through IEP exhibits a unique behavior of initial increase followed by decrease, which contrasts with the ECP process [2].

Building upon preliminary research, this study centers on experimentally investigating the evolution of the NiP plating surface during IEP, with the ultimate aim of attaining sub-nanometer surface roughness (Sa $<$ 0.2 nm) for its commercial applications. The study also delves into the anodic polarization curve of NiP plating, the impact of voltage in the polishing process, and the formation of a passivation layer on NiP plating when subjected to various electrolytes. Furthermore, the investigation explores the relationship between surface morphology evolutionary process, material removal rate (MRR), and average surface roughness (Sa roughness) with different etching current.

2. Experimental setup

2.1. Isotropic etching polishing (IEP) of the NiP plating

For the present investigation, the commercially available electroless nickel plating (NiP plating) with a 10 mm diameter and a thickness ranging from 100 to 150 μm was applied to 304 stainless steel substrates. Electropolishing was conducted on the electroless nickel-plated surface facing the anode, while precautionary measures were taken to safeguard the side and back faces with silicone rubber insulation. To eliminate the rough marks made by machining process, the substrates were treated with SiC sandpapers (#800). Subsequently, the substrates were subjected to ultrasonic cleaning in ethyl alcohol and deionized water for a duration of 5 mins each, aiming to effectively eliminate any potential contaminants present. Fig. 1 illustrates the setup configured in this experiment of research.

For the electrochemical etching process, a glass beaker was utilized, and the electrolyte employed in this study consisted of a mixture comprising concentrated sulfuric acid and methanol. The counter electrode was chosen to be a platinum sheet with dimensions of 20 mm × 20 mm, while the working electrode consisted of the electroless NiP plating

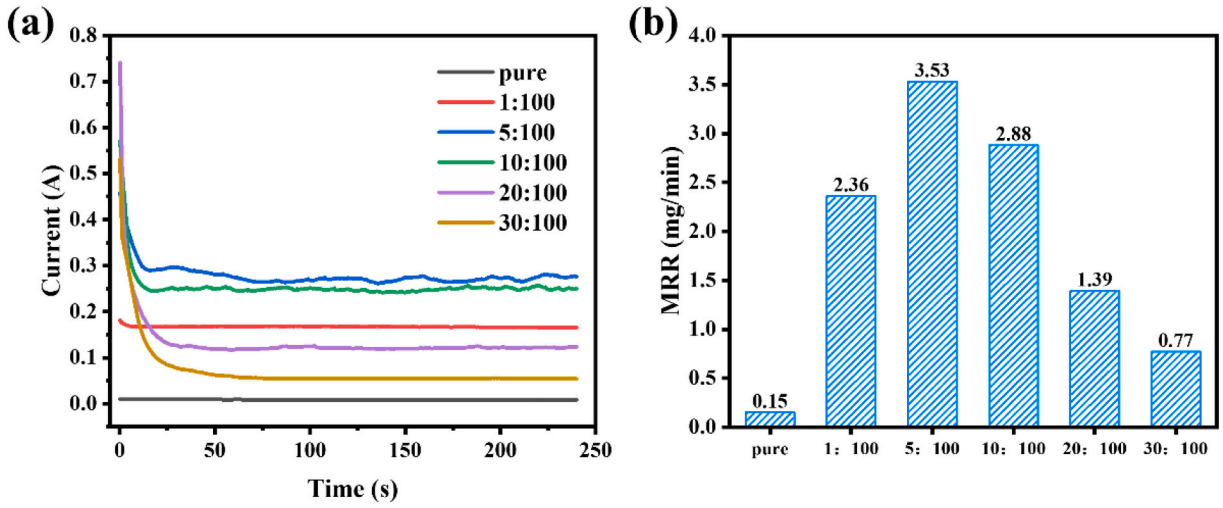

Fig. 7. (a) The current-time curves of various electrolyte ratios, (b) Material removal rates of different electrolyte ratios.

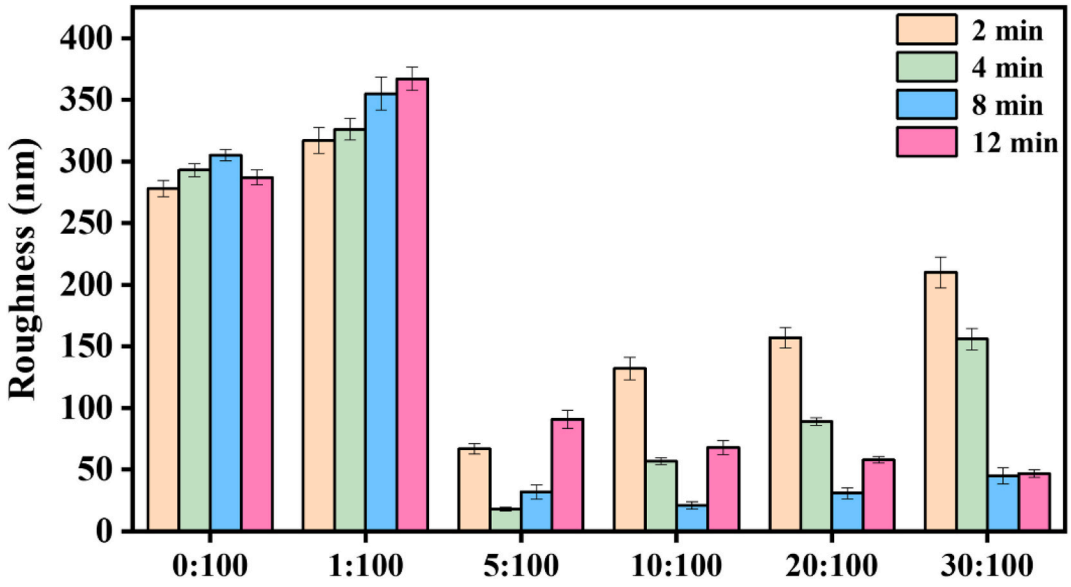

Fig. 8. Roughness variations were observed with respect to polishing time (2, 4, 8 12 min) using WLI under different electrolyte conditions (the ratios of H_2SO_4 to CH_3OH were 0:100, 1:100, 5:100, 10:100, 20:100 and 30:100).

on the 304 stainless steel substrates. The copper wire was connected to the tail of the substrate, with the exception of the polished NiP plating surface, which was covered with insulating silicone rubber. The electrochemical etching was performed by using the KEITHLEY 2280S to provide electric current. The distance of 20 mm between the center of the substrate and the counter electrode was consistently upheld. After the completion of the anodic etching process, the samples underwent a thorough rinse with water and were subsequently dried using N_2 gas. All experiments were conducted under standard ambient room temperature conditions, unless otherwise specified.

The polishing electrolyte employed in this study comprises concentrated sulfuric acid (H_2SO_4–97 %) and methanol (CH_3OH-99.5 %). Each component of the electrolyte fulfills distinct roles: (i) H_2SO_4 functioned for anodic surface passivation and etching [39], and (ii) CH_3OH acted to destabilize the passivation layer [23]. The collective reactions occurring within the reaction cell can be succinctly summarized as follows:

$$\text{Cathode}: 2nH_2SO_4 + 2ne^- \rightarrow nSO_2 + nSO_4{}^{2-} + 2nH_2O \quad (1)$$

$$2nH^+ + 2ne^- \rightarrow nH_2 \quad (2)$$

$$\text{Anode}: n\text{Ni (s)} \rightarrow n\text{Ni}^{2+} + 2ne^- \quad (3)$$

$$2nH_2O \rightarrow 4nH^+ + nO_2 + 4ne^- \quad (4)$$

2.2. Characterization

The properties of electrochemical processes were assessed through an electrochemical workstation (CHI660e, Shanghai Chenhua Instrument Co., LTD). The workpiece served as the anode and established a connection with the positive terminal of a direct current power source. Throughout the experiments, a fixed distance of 20 mm was preserved between the cathode and anode. During each trial, both the voltage and current values were meticulously recorded and subsequently transferred to a computer for further analysis and interpretation. Surface morphology analysis was conducted before and after the polishing process by using scanning electron microscopy (SEM, ZEISS Merlin) and laser scanning confocal microscopy (LSCM, Keyence VK-X1000). To gain insights into the surface roughness, atomic force microscopy (AFM, Bruker Edge) and scanning white light interferometry (Taylor Hobson

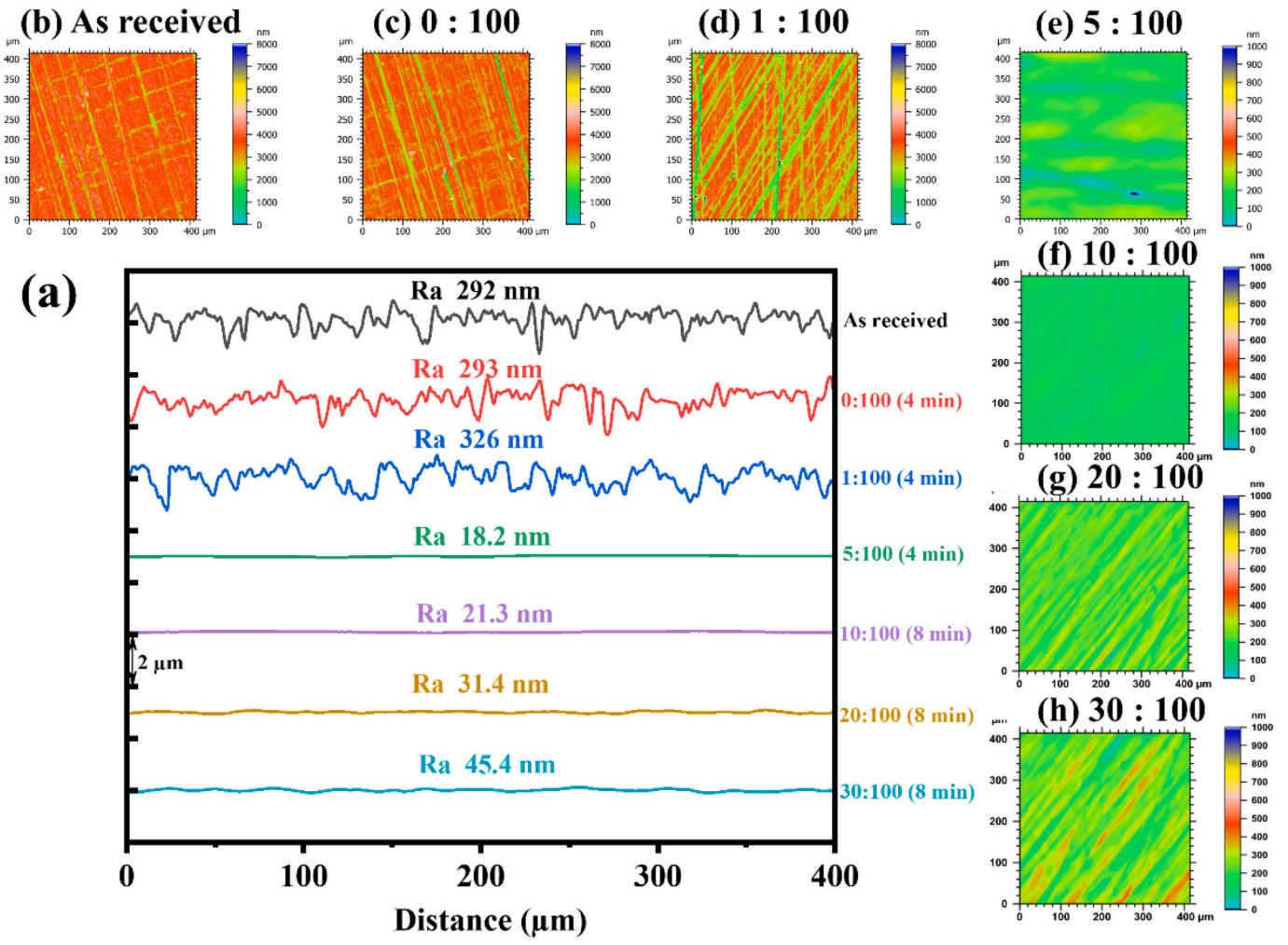

Fig. 9. Characterization of WLI topographical profiles and Ra roughness variation in NiP plating (a), As received (b) and after polishing at 7 V voltage in electrolytes ratio were 0:100 for 4 min (c), 1:100 for 4 min (d), 5:100 for 4 min (e), 10:100 for 8 min (f), 20:100 for 8 min (g), 30:100 for 8 min (h).

M112-4449-02 CCI HD) were employed. In addition, the material removal rate (MRR) was determined by precisely measuring the variation in substrate mass before and after isotropic etching polishing (IEP) using a high-precision balance (Mettler Toledo, ME203).

3. Results and discussions

3.1. Chemical composition of the NiP plating

Electroless nickel plating can be classified into the low phosphorus electroless nickel plating ($P \leq 5$ wt%), the medium phosphorus electroless nickel plating (5 wt% $< P <$ 8 wt%) and the high phosphorus electroless nickel plating ($P \geq 9$ wt%) [12]. The composition of the electroless nickel plating layer significantly influences its structural and property characteristics, with the phosphorus content playing a predominant role in determining these attributes. With the rising of phosphorus content in the plating, the micro-structure transfers from crystalline to microcrystalline and finally forms amorphous state. The high phosphorus electroless nickel plating possesses the excellent corrosion resistance and machinability, which is suitable for the preparation of the super-smooth optical instruments coating [4]. The surface of the original workpiece exhibited residual knife marks following cultivation, as illustrated in Fig. 1b. The chemical composition (wt%) of the NiP plating utilized in this investigation was measured analytically using an energy dispersive spectrometer (EDS) coupled with a scanning electron microscope (SEM, ZEISS Merlin). The red wire frame in Fig. 2a was analyzed by EDS surface scan, as shown in Fig. 2b. The results of the analysis shows that Ni element and P element are evenly distributed on the surface. The energy spectrum of element content distribution is shown in Fig. 2c, the NiP plating has a phosphorus atomic ratio of 8.53 %, closing to the high phosphorus electroless nickel plating. Fig. 2d presents the X-Ray Diffraction (XRD) patterns of the electroless nickel plating sample, obtained by scanning with Cu-Kα radiations at a step size of 0.02°. The XRD analysis was performed under operating conditions of 45 kV and 200 mA. The diffraction peak is the steamed bun peak, indicating the surface NiP plating is amorphous [12,18].

3.2. Anodic dissolution behavior

During the initial stage of the study, the electrochemical polarimetric curve of the NiP plating was determined. This curve serves as a valuable tool for elucidating the fundamental principles of metal etching, uncovering the underlying mechanisms governing the etching process, and providing a preliminary assessment of the optimal voltage range for polishing [9]. Fig. 3a exhibits the polarized curve of the NiP plating in the electrolyte containing a volume ratio of 10:100 (H_2SO_4 to CH_3OH). During the anode polarized area, the polarized curve can be classified into two distinct states. Within the voltage range of 0 to 3.5 V, commonly referred to as the etching region, the current density demonstrated a pronounced exponential increase concomitant with the applied voltage. This behavior signified that the workpiece underwent direct dissolution, with the overpotential functioning as the activating

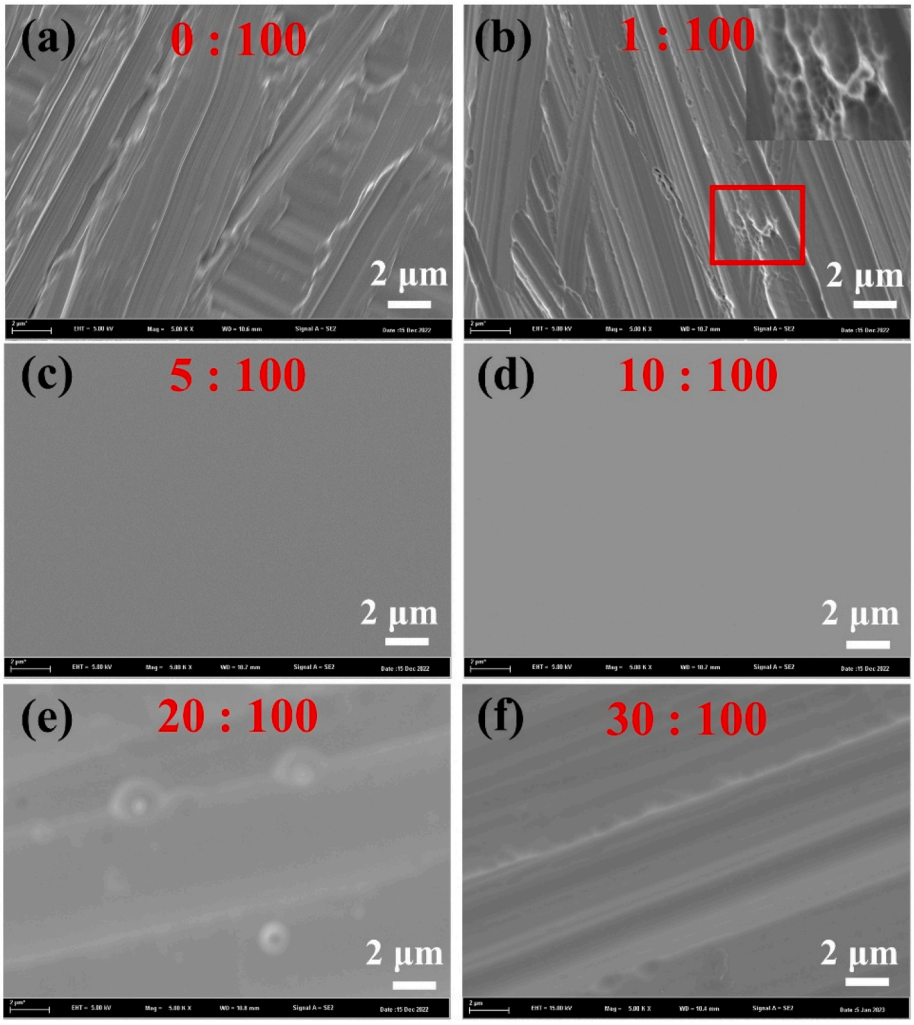

Fig. 10. SEM surface morphologies of NiP plating polished at 7 V voltage for 240 s in electrolyte ratios were (a) 0:100, (b) 1:100, (c) 5:100, (d) 10:100, (e) 20:100, (f) 30:100.

energy for the etching process [7]. In other words, anodic product diffusion rate in the bulk electrolyte was rapid without accumulation on the workpiece surface. Within the voltage range of 3.5 V to 9 V, called limited current plateau region, the current density exhibited a notable constancy as the voltage increased. This observation signifies that the dissolution of the NiP plating was effectively regulated by the mass transfer process occurring within the electrolyte. In this region, the accumulation of the anodic products causing the appearance of a stable and passivation film on the workpiece. Consequently, the dissolution of the NiP plating falls under the category of mass transfer polarization [40]. The polarization effect on the NiP plating under various applied voltages was investigated. Fig. 3b illustrates the time-current curves acquired at voltage range of 2 V and 7 V. Under a voltage of 2 V, the anodic product diffused rapidly, and the dissolution rate of the material was solely influenced by the activation polarization, resulting in almost no change in the current. The concentration of anodic products showed no significant difference between the surface and bulk fluid, indicating the absence of mass transfer polarization and keeping the current constant over time. At a voltage of 7 V, the current exhibited a significant drop within the initial 20 s. The higher voltage led to an accelerated workpiece material removal rate, causing a substantial accumulation of the anodic products on the anodic surface as they were unable to diffuse in time [36]. As the polishing time increased, a balance between the product diffusion and material removal rate was achieved. Moreover, the emergence of a passive oxide layer on the anode efficiently promoted the electrochemical polishing process on the surface of workpiece.

For purpose of observing the evolution of the etching pits, the as-received NiP plating was sanded with # 800 sandpaper. The surface morphologies observed following a 1-s etching duration at a voltage of 2 V were depicted in Fig. 4a. The surface exhibited only scratches resulting from sandpaper grinding, and no round etching pits were detected. This indicated that the surface morphology of NiP plating remained unchanged for the short etching time under a lower voltage. Following an etching duration of 120 s at the voltage of 2 V (as depicted in Fig. 4b), the scratches on the workpiece surface exhibited a reduction in depth, becoming shallower than before. Additionally, a few circular corrosion pits were observed, randomly distributing across the surface. When an applied potential of 2 V was employed, the surface of the processed NiP plating underwent etching without achieving a polished state. Differently, irregularly distributed etching pits were observed on the surface of workpiece after processing for a duration of 1 s at the voltage of 7 V, as depicted in Fig. 4c. Due to the increase of voltage, the material dissolution rate increased, which enhanced the formation of passivation film. Because the NiP plating was amorphous, the dissolution ratio of the material in all directions was consistent, resulting in the formation of isotropic corrosion pits. The scratch edge was higher with a thinner passivation film, the corrosion pits concentrated at the scratch edges, as shown in Fig. 4c partial enlarged drawing. After etching for 120 s at the voltage of 7 V (Fig. 4d), the surface turned smooth and the surface roughness of the plating decreased to 0.225 nm in the area of 20 µm

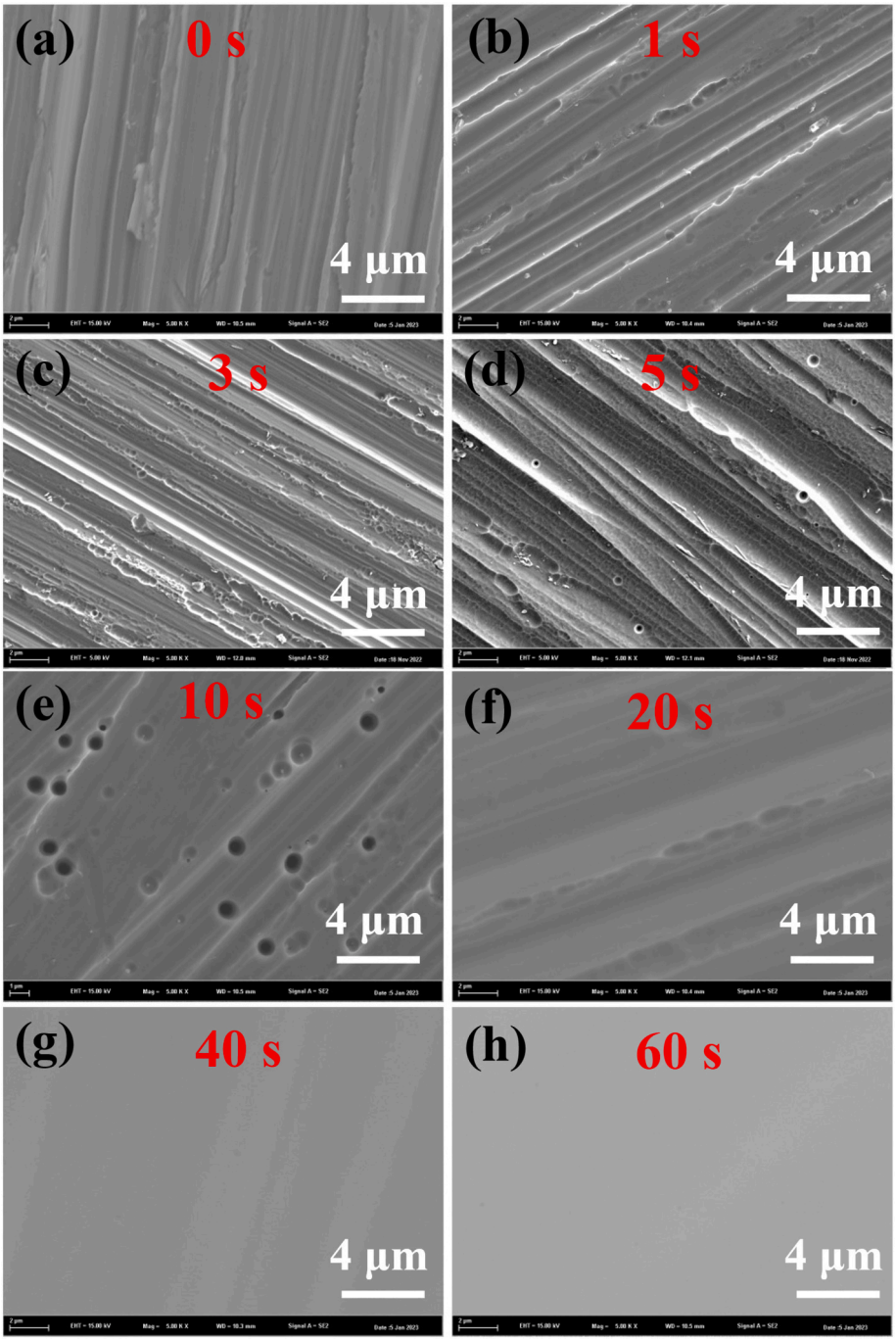

Fig. 11. Surface morphologies of NiP plating after IEP in electrolyte with a volume ratio of 5:100 at 7 V for different etching durations.

(Fig. 4e). The reduction of roughness indicated that the electrochemical polishing voltage needed to be in the limited current plateau region, in which mass transfer polarization occurs. During this condition, the surface of the workpiece rapidly formed a passivation layer, and the isotropic corrosion pits preferentially appeared on the surface bulges.

3.3. The effect of voltage on ECP

The impact of voltage on the polishing result was investigated by examining the surface morphology of the NiP plating across various voltage levels (ranging from 1.5 V to 18 V) using LSCM, as illustrated in Fig. 5. The surface of the NiP plating displayed knife lines and defects resulting from gas evolution during the production process, as depicted in Fig. 5a. When a voltage of 1.5 V was applied, electrochemical dissolution of the NiP plating took place, with preferential dissolution occurring at the defects present on the original surface. When the voltage was increased to 3 V, the electrochemical dissolution rate accelerated significantly, leading to the dissolution of the original knife lines and defects. However, due to the absence of a dense passivation layer and the occurrence of pure electrochemical corrosion, numerous small-sized corrosion pits appeared on the surface, as depicted in Fig. 5c. When the voltage ranged from 5 V to 12 V (Fig. 5d and e), the knife lines and defects on the material surface disappeared, indicating a smooth NiP plating surface. Similarly, dense pits that compromised the surface integrity appeared when the applied potential was sufficiently high, such as 14 V. Moreover, a massive number of bubbles appeared on the surface of the NiP plating during the experiment, and their release caused the formation of larger spherical holes on the workpiece. As the

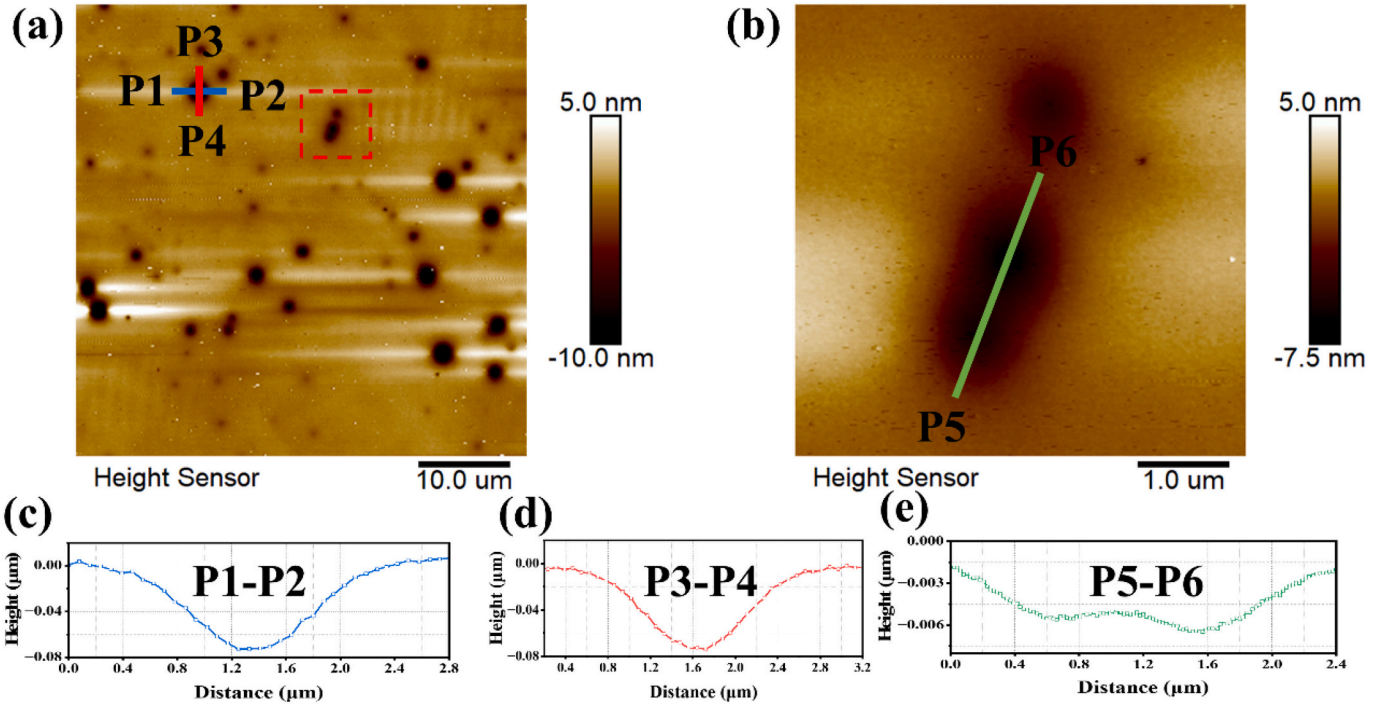

Fig. 12. Morphological analysis of isotropic etching pits in NiP plating via AFM in 5:100 H_2SO_4 electrolytes at 7 V for a duration of 10 s: (a) overall morphology, (b) red wireframe enlarged area, (c. d. e) cross-sectional schematics of etching pits. (For interpretation of the references to colour in this figure legend, the reader is referred to the web version of this article.)

potential increased, the amount of gas evolution also increased. Fig. 5(f-h) illustrates the observation of not only numerous corrosion pits but also the presence of holes resulting from bubble formation. The continuous formation and precipitation of bubbles disrupt the stability of the passivation layer. These bubbles create localized disturbances in the electrolyte, accelerating the rate of electrochemical dissolution. Consequently, this process leads to the formation of concave cavities on the surface. The number of larger spherical holes increased with the potential. To achieve a NiP plating surface that is both smooth and devoid of pits, the applied potential must fall within an intermediate range of 4–12 V.

Drawing upon the synthesis of the aforementioned studies, it becomes apparent that voltage assumes a pivotal role in the process of electrochemical polishing. The voltage directly impacts the polarization state of the NiP plating, specifically affecting surface polishing in the mass transfer polarization region. Fig. 6 depicts the current density-voltage curve of the Isotropic Etching Polishing (IEP) process for the NiP plating. According to the polishing effect and experimental phenomenon, the current density-voltage curve was preliminarily divided into three stages, which are the etching stage, the limited current plateau stage and the gas evolution stage, similar to Jacquet's theoretical model [11]. In the etching region, the workpiece underwent the direct dissolution. Due to the presence of a mechanically worked surface, the NiP plating surface in this specific region exhibited the formation of circular pits, accompanied by discernible scratches that persisted on the material's surface. Moving to the limited current plateau region, the current density remained nearly constant even as the voltage increased. At this stage, a balance existed between the anodic formation and diffusion rate, causing the appearance of a stable passivation film on the workpiece. Upon entering the gas evolution region, the stability of the passivation film was perturbed with the progressive rise in voltage, resulting in anodic dissolution accompanied by the generation of oxygen. The accumulation and growth of oxygen bubbles on the workpiece surface ensued, ultimately accumulating and subsequently releasing, hastening the rate of electrochemical dissolution, thereby causing pronounced holes to form on the workpiece surface.

3.4. The effect of electrolyte concentration

The electrolyte serves as the medium for the material transfer and heat exchange in the electrochemical polishing process, and its composition ratio significantly impacts the polishing outcome. The concentration of sulfuric acid determines the viscosity, electrical conductivity, and oxidation characteristics of the electrolyte. Fig. 7a shows the current-time curves with different ratios of H_2SO_4 to CH_3OH (0:100, 1:100, 5:100, 10:100, 20:100, 30:100) at 7 V constant voltage. When the electrolyte ratio was 0:100, the current was close to 0 A. Because of the low conductivity of pure methanol solution, the workpiece hardly produced electrochemical dissolution. As the ratio of H_2SO_4 to CH_3OH was 1:100, the current decreased slightly within a short time and then remained at 0.17 A. The low concentration of sulfuric acid resulted in an uneven passivation film on the surface of the NiP plating, causing inconsistent electrochemical dissolution of the workpiece. Furthermore, as the sulfuric acid content increased, a significant reduction in current was observed, indicating the occurrence of the mass transfer polarization during the polishing process. As the ratio of H_2SO_4 to CH_3OH was 5:100, the polishing current stabilized at 0.27 A. With the further increased of sulfuric acid content, the polishing current decreased gradually. As the ratio of H_2SO_4 to CH_3OH were 10:100, 20:100 and 30:100, the corresponding polishing current were 0.25 A, 0.13 A and 0.06 A. It indicated that the passivation film thickened and the conductivity of the electrolyte decreased. The material removal rates of various electrolyte ratios were shown in Fig. 7b. As the ratio of H_2SO_4 to CH_3OH were 0:100, 1:100, 5:100 10:100, 20:100 and 30:100, the corresponding Material removal rates were 0.15, 2.36, 3.53, 2.88, 1.39 and 0.77 mg/min. Therefore, when the electrolyte composition ratio was 5:100, the NiP plating had the highest polishing efficiency.

The formation of a stable passivation layer on the surface of the anode is crucial for the process of electrochemical polishing. This passivation layer has a complex composition, primarily consisting of sulfuric acid molecules, metal ions, and organic matter. Additionally, it possesses high viscosity and high resistance properties, contributing to its stability and durability. When the solution lacks sulfuric acid, the

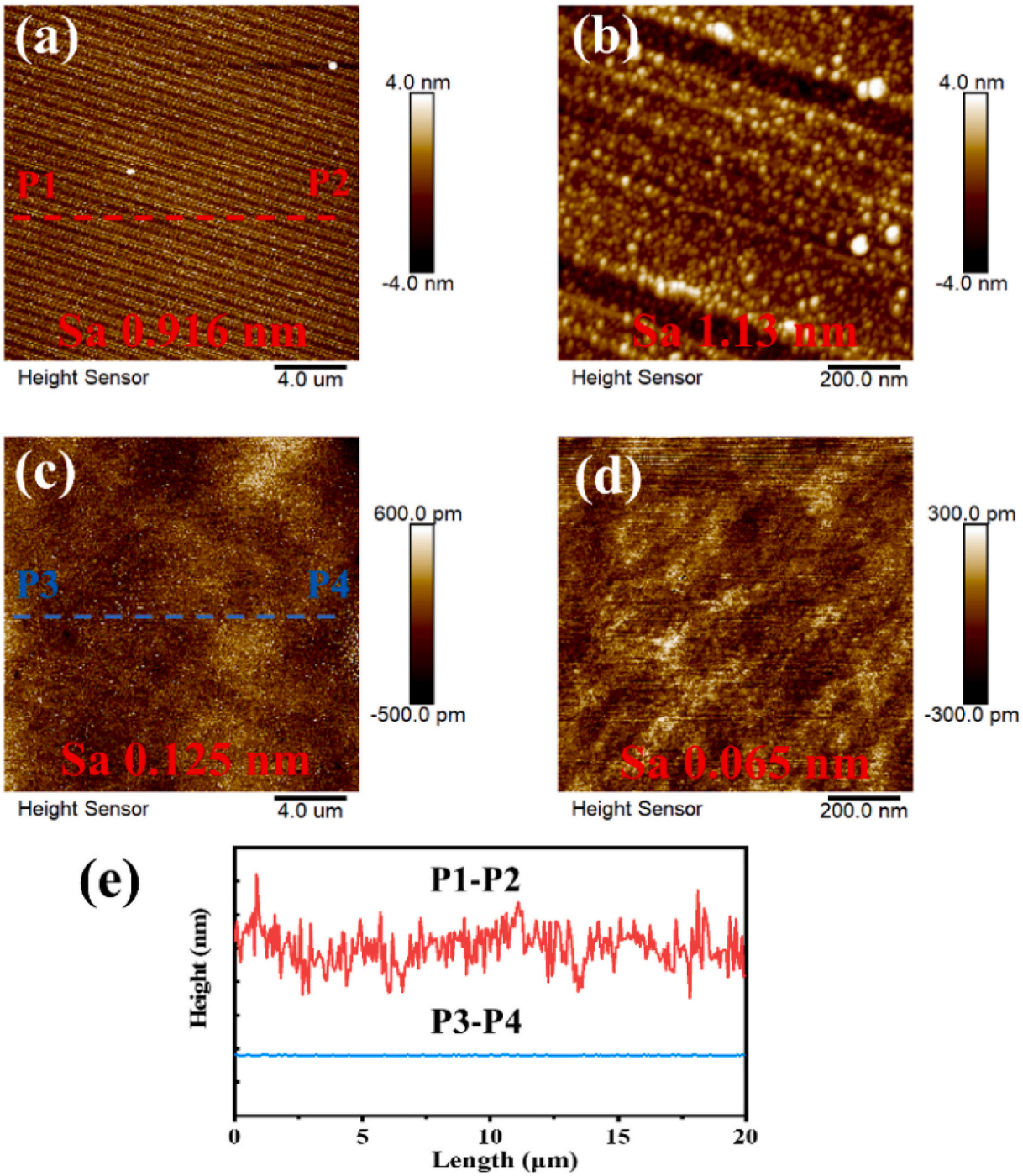

Fig. 13. Surface morphologies and Sa roughness measured by AFM, and graphs of NiP plating before (a, b) and after 240 s of IEP at 7 V in electrolyte comprising a volume ratio of H_2SO_4 to CH_3OH of 5:100 (c, d).

electrolyte exhibits significantly low conductivity, leading to minimal electrochemical reactions occurring within the NiP plating. However, when the sulfuric acid content ratio is adjusted to 1:100, as the polishing time is prolonged, the roughness of the workpiece actually increases. This indicates that the addition of sulfuric acid enhances the conductivity of the electrolyte. However, due to the low sulfuric acid content, a stable passivation layer cannot be formed. As a result, no significant polishing occurs under these conditions. When the sulfuric acid ratio exceeds 1:100 (the ratios of H_2SO_4 to CH_3OH were 5:100, 10:100, 20:100 and 30:100), a notable reduction in roughness is observed, indicating that an increase in sulfuric acid content facilitates the formation of a more effective passivation layer. In the same electrolyte ratio, the roughness exhibits an initial decrease followed by an increase as the polishing time progresses. This can be attributed to the gradual consumption of active ingredients in the electrolyte and the subsequent instability of the passivation film. Consequently, the roughness tends to increase over time.

Fig. 9 illustrates the minimum roughness of the NiP plating at various electrolyte concentrations. When the sulfuric acid content is very low, such as in ratios of 0:100 or 1:100, the surface scratches on the workpiece do not disappear, and the roughness does not exhibit significant changes. This indicates that the low sulfuric acid concentration is

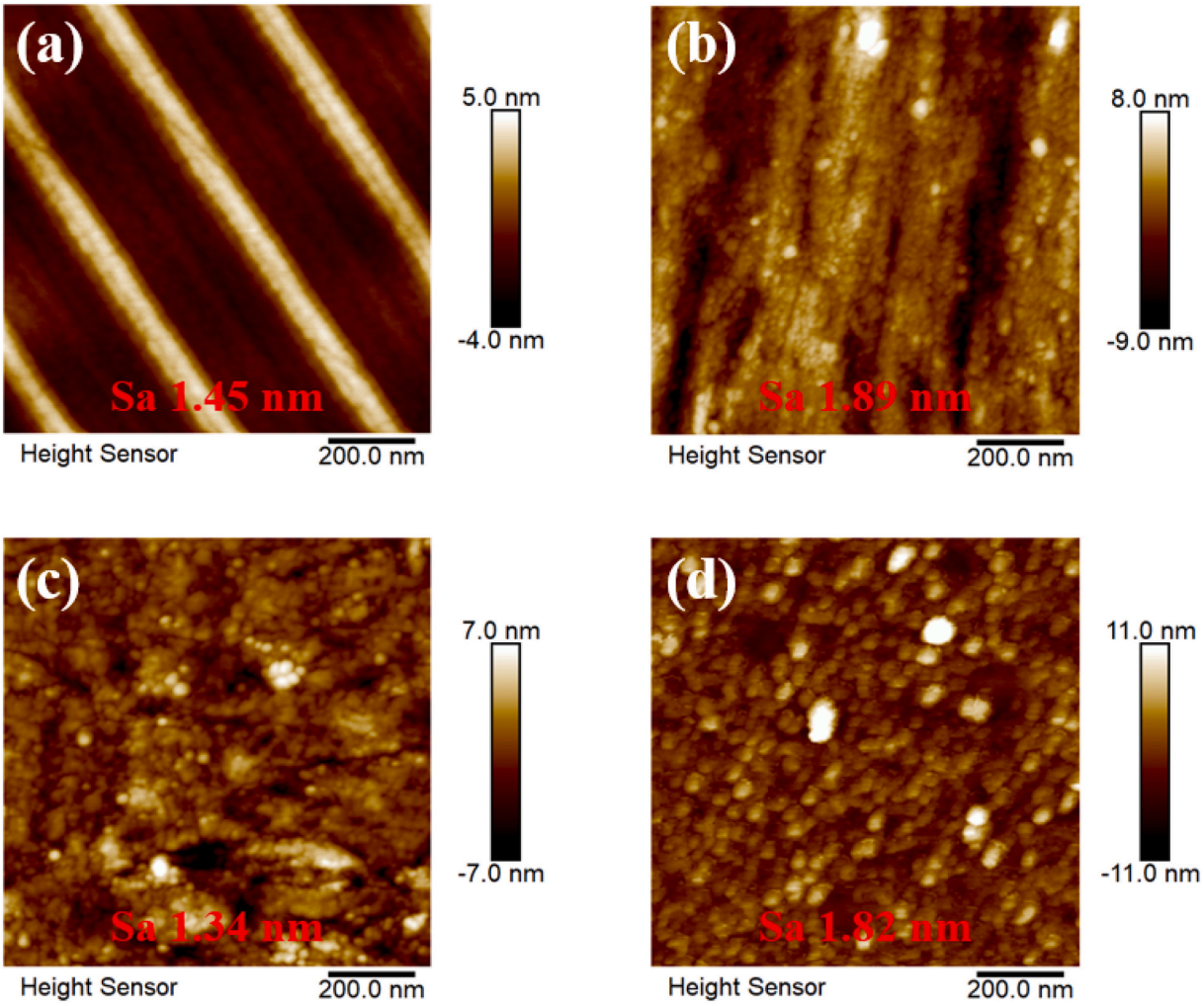

Fig. 14. Surface morphologies and Sa roughness by AFM, and pictures of NiP plating after SPDT (a), magnetorheological finishing (MRF) with diamond (b), magnetorheological finishing (MRF) with CeO_2 (c), Small-tools Polishing (STP) (d).

insufficient to effectively remove or modify the surface defects, resulting in limited improvement in roughness. Higher sulfuric acid concentrations, exceeding 5:100, and polishing the nickel-phosphorus alloy at 7 V voltage, result in a trend where the roughness initially decreases and then increases with prolonged polishing time. The different sulfuric acid content directly affects the electrolyte's polishing ability. At an electrolyte ratio of 5:100, the minimum roughness of 18.2 nm can be achieved in just 4 mins. However, as the electrolyte ratio increases, it takes longer to reach the lowest roughness. The composition of the electrolyte directly impacts the formation and stability of the plating film, thereby influencing the efficiency of the polishing process and the attainment of the minimum roughness.

The micromorphology of the workpiece polished in different electrolytes was shown in Fig. 10. Fig. 10a only showed scratches, which verified the absence of an electrochemical reaction in the pure methanol solution for the NiP plating. Fig. 10b demonstrated that at a sulfuric acid ratio of 1:100, there was intense electrochemical corrosion of the NiP plating at the edges of the scratches, resulting in the formation of the dense corrosion pits in the red area. The smooth and flat surface of the material in Fig. 10c and d indicated that the NiP plating underwent the electrochemical polishing. Compared to the results in Fig. 8, the electrolyte with a volume ratio of 5:100 exhibited a higher polishing efficiency. Fig. 10e and f showed the presence of shallow scratches and isotropic corrosion pits, indicating the existence of a passivated film on the surface and the occurrence of the isotropic electrochemical polishing. However, the high sulfuric acid content resulted in ascending viscosity and notable reduction in the diffusion rate of anodic products. Thus, the electrolyte composition ratio of IEP technology must fall within a certain range to guarantee the formation of a passivation film and sufficient diffusion rate of substances.

3.5. Isotropic etching polishing mechanism of the NiP plating

Taking advantage of the isotropic etching behavior characteristic of the NiP plating, the isotropic etching polishing (IEP) of the NiP plating was carried out under meticulously optimized conditions. This endeavor aimed to explore and analyze the progression of the morphology of surface, roughness of surface, and efficiency of polishing throughout the etching process. The NiP plating underwent etching at a consistent voltage of 7 V, with diverse durations ranging from 0, 1, 3, 5, 10, 20, 40, to 60 s, aiming to investigate the evolutionary changes in surface morphology. Fig. 11a depicted the numerous scratches on the original substrate surface, resulting from the sanding process. After etching for a duration of 1 s, tiny isotropic etching pits emerged on the scratches of surface (Fig. 11b). Due to the higher position of the scratch edge with a thinner passivation film, isotropic etching pits were more likely to occur. After etching for a duration of 3 s, the number of isotropic etching pits on the scratches continuously increased and partial isotropic etching pits started intersecting (Fig. 11c). After etching for a duration of 5 s (Fig. 11d), the surface of the workpiece was full of isotropic etching pits,

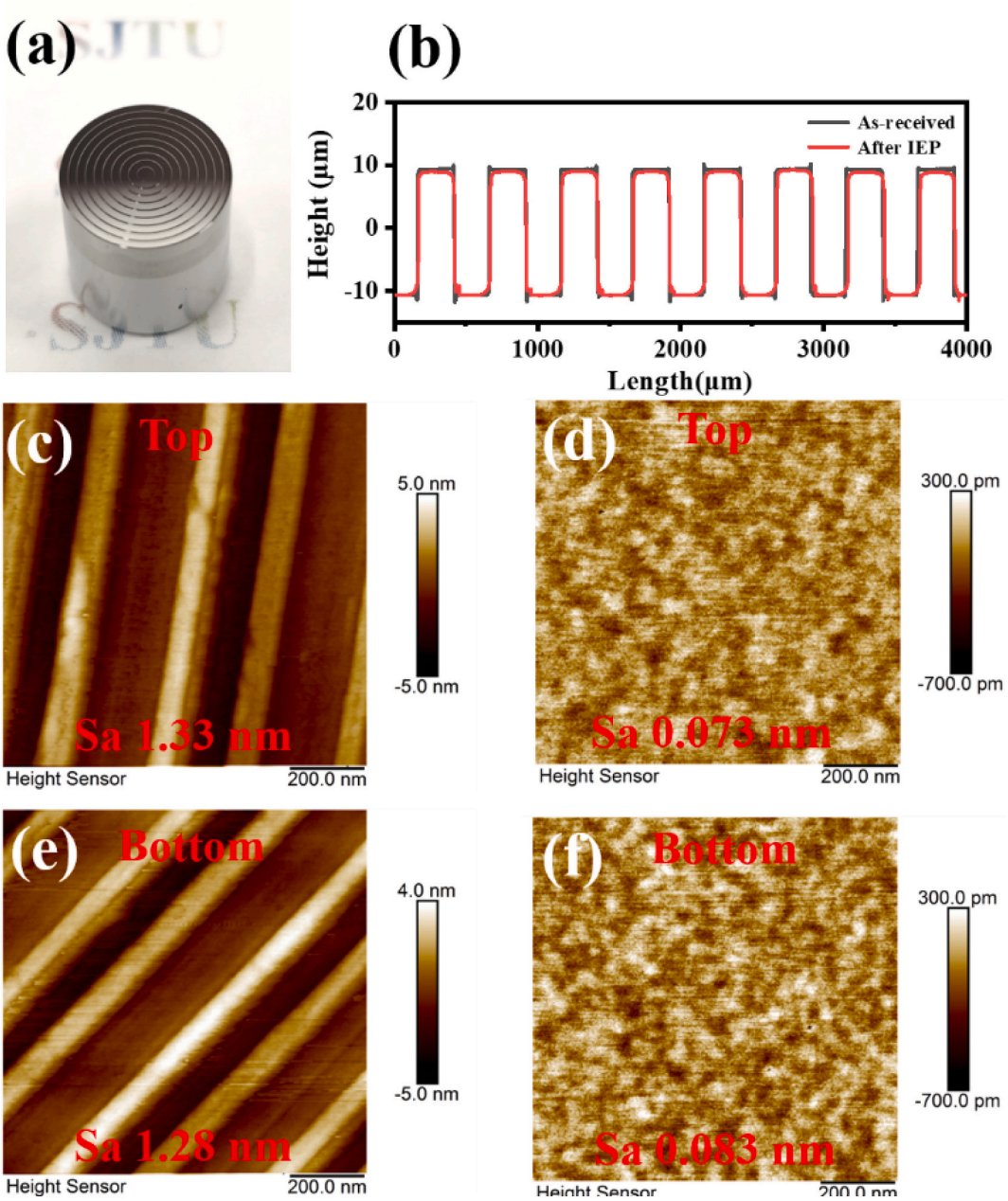

Fig. 15. The image of grating microstructure (a), surface profile of the grating microstructure before and after IEP by WLI (b), the top of grating microstructure before (c) and after (d) IEP, the bottom of grating microstructure before (e) and after (f) IEP with 240 s at 7 V in 5:100 H_2SO_4 electrolytes.

and the adjacent corrosion pits were mixed. After etching for a duration of 10 s (Fig. 11e), the depth of the scratches decreased, and larger round corrosion pits formed. The combination of etching pits resulted in the formation of the smooth basin structures. After etching for a duration of 20 s (Fig. 11f), the isotropic etching pits continually grew and the scratches became smoother. After etching for a duration of 40 s, the residual areas were basically removed, but a small number of waviness still were observed, as shown in Fig. 11g. Eventually, after 60 s of etching, the surface became remarkably flat, exhibiting no signs of waviness (Fig. 11h). In summary of the results depicted in Fig. 11, the process of surface smoothing demonstrated strong concordance with the mechanism of isotropic etching polishing as proposed.

The etching pits emerged on the NiP plating after processing for a duration of 10 s at a voltage of 7 V were measured using AFM, as depicted in Fig. 12. Fig. 12a illustrated the random distribution of etching pits across the substrate surface, wherein certain pits exhibited interconnections with neighboring pits. In Fig. 12b, one can observe the presence of neighboring pits, each possessing a diameter of approximately 1 μm. Evidently, the elimination of the NiP plating was accomplished through the interconnection of these adjacent corrosion pits. As the radius of the isotropic corrosion pits increased, the surface roughness of the workpiece increased. Fig. 12c and d presented the semicircular horizontal and vertical profiles of an etching hole in Fig. 12a, demonstrating the etching pits were symmetrical sphere. Fig. 12e showed the process of the adjacent etching pits, indicating that the material removal was realized by the growth and merging of etching pits. Since the crystal structure of the NiP plating was amorphous, the material removal rate was uniform in all directions, and no anisotropic corrosion pits were observed.

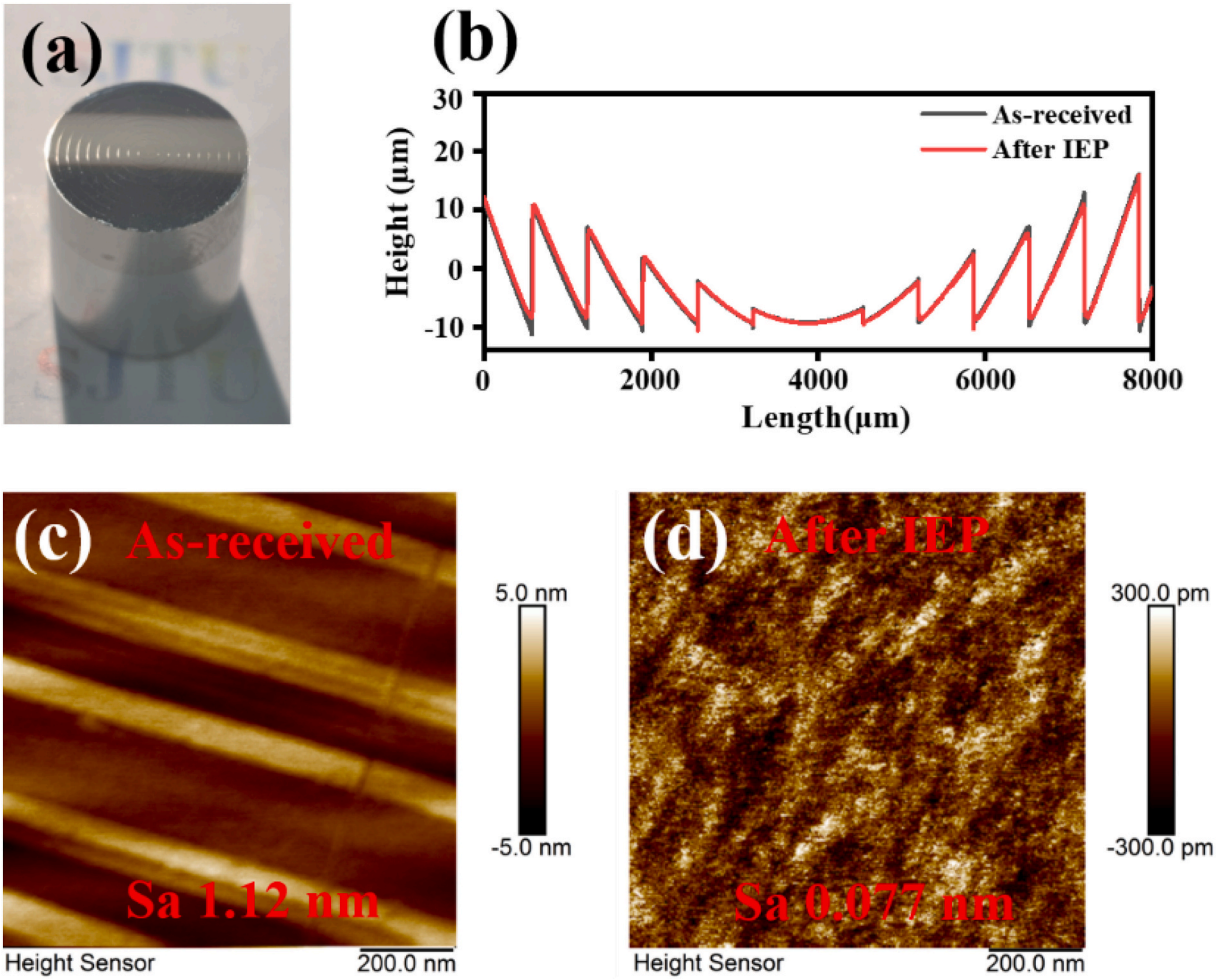

Fig. 16. The image of Fresnel lens (a), surface profile of the Fresnel lens before and after IEP by WLI (b), the surface morphologies and Sa roughness by AFM before (c) and after (d) IEP with 240 s at 7 V in 5:100 H_2SO_4 electrolytes.

3.6. Comparison of surface roughness of the NiP plating by using IEP and other polishing methods

Fig. 13 showcases the atomic force microscopy (AFM) graphs portraying the roughness and sectional profiles of two distinct surfaces: one machined via ultra-precision cutting, and the other processed through isotropic etching polishing (IEP). After machined by Single Point Diamond Turning (SPDT), obvious knife lines were observed on the NiP plating surface, the Sa roughness of different test ranges were 0.916 nm (20 × 20 μm) and 1.13 nm (1 × 1 μm). Fig. 12c and d showed that the Sa roughness drastically decreased to 0.125 nm (20 × 20 μm) and 0.065 nm (1 × 1 μm) after carrying out the IEP for 240 s. The achieved sub-nanometer surface roughness of the NiP plating demonstrates that IEP is a viable polishing technique for achieving ultra-precision in the manufacturing.

For comparison, the NiP plating was machined by using four commonly used ultra-precision polishing methods. Fig. 14 showed the results of surface morphologies and Sa roughness of surface of NiP plating measured by AFM. Fig. 14a showed that the Sa roughness of NiP plating was 1.45 nm (1 × 1 μm) after carrying out SPDT while knife lines were obviously observed on the surface. After polished by the MRF with diamond granules, Fig. 14b showed that the Sa roughness of NiP plating was 1.89 nm (1 × 1 μm). Fig. 14c showed the result of the morphology of the surface of NiP plating after using MRF with CeO_2 granules, and it displayed that the Sa roughness decreased to 1.34 nm (1 × 1 μm). Ultimately, the Sa roughness of surface of NiP plating was 1.82 nm (1 × 1 μm) after using STP polishing technique (abrasive particles: CeO_2; average diameter of abrasive: 0.15 μm; polishing pressure: 0.04 Mpa; rotation speed: 80 rpm; polishing pad: damping cloth W60) as depicted in Fig. 14d. The results illustrated that compared to polishing methods such as MRF and STP, the IEP polishing method can achieve the lower surface roughness without introducing additional contact stress to the polished surface.

3.7. The results of the grating microstructure by IEP

The grating microstructure components were widely used in the optical field. The difficulty in polishing lied in the requirement to simultaneously maintain the microstructure shape and achieve the surface roughness below 0.1 nm. Contact polishing methods such as MRF and STP achieved the material polishing through shear stress, which inevitably damaged the shape of the microstructure. IEP, as a non-contact polishing method, was theoretically suitable for ultra-smooth polishing of grating microstructures due to the good accessibility of its solution. Fig. 15a showed the physical image of the grating microstructure. After IEP, it can be observed that the microstructure at the micron-scale is effectively preserved (Fig. 15b), indicating that IEP has good shape-preserving ability. After AFM measurement, the results revealed a notable decrease in the surface roughness of both the upper and lower surfaces of the grating microstructure, measured at 0.073 nm and 0.083 nm, respectively. (Fig. 15d, f), respectively. The experimental results indicated that through IEP, the grating microstructure can

achieve ultra-precision surface characterized by a surface roughness below the threshold of 0.1 nm. Additionally, this process demonstrated an exceptional capability for preserving the shape and integrity of the surface features.

3.8. The results of the Fresnel lens by IEP

The Fresnel lens components found extensive applications in the optical field. Fig. 16a depicted the physical image of the Fresnel lens. After IEP, it became evident that the microstructure at the micron-scale was effectively preserved (Fig. 16b), signifying IEP's commendable shape-preserving ability. Subsequent AFM measurements revealed a reduction in surface roughness of the Fresnel lens from 1.12 nm (Fig. 16c) to 0.077 nm (Fig. 16d). These experimental results demonstrated that IEP facilitated the attainment of the ultra-smooth surfaces on the Fresnel lens, exhibiting a surface roughness below 0.1 nm and exceptional shape preservation.

4. Conclusions

In this study, an analytical investigation of IEP of the NiP plating is proposed. The study confirms the validity and mechanism of the IEP. Specifically, it investigates the alterations in the surface morphology, surface roughness, and electric current at varying voltages. Moreover, the impact of electrolyte content on the polishing effect is thoroughly examined. The following conclusions could be summarized from this investigation:

(1) As a non-contact and ion-diffusion electrochemical polishing technology, The efficacy of IEP for the purpose of surface smoothening in NiP plating has been substantiated. The knife lines made by ultra-precision cutting disappeared, and a sub-nanometer roughness of 0.065 nm was acquired by IEP in 4 mins.
(2) Based on the influence of voltage on the polarization condition and surface morphology, IEP of the NiP plating with various applied voltages were classified into 3 distinct stages: the etching stage, the limited current plateau stage and the gas evolution stage. The voltage range within where the NiP plating exhibits a polishing effect is approximately 4 V to 12 V.
(3) Material removal occurred through the merging and growth of adjacent etching pits, which were formed by the breakdown of the passivation layer. Super-smooth polishing of the NiP plating surface was achieved only when a stable and dense passivation film was formed.
(4) Compared to other ultra-precision polishing method, the IEP has the better performance in optimizing the surface roughness of the NiP plating. IEP has a good shape-preserving ability and can maintain the shape of both the grating microstructure and Fresnel lens at the micron scale without damage.

Declaration of competing interest

The authors unequivocally declare that there are no discernible financial conflicts of interest or personal relationships that could have influenced the impartiality or credibility of the findings presented in this academic article.

Acknowledgements

This work was Supported by the National Key Research and Development Program of China under Grants 2022YFB3403301.

References

[1] Abbott AP, Capper G, McKenzie KJ, Ryder KS. Voltammetric and impedance studies of the electropolishing of type 316 stainless steel in a choline chloride based ionic liquid. Electrochim Acta 2006;51:4420–5. https://doi.org/10.1016/j.electacta.2005.12.030.
[2] Ajmal KM, Yi R, Zhan Z, Ji J, Zhang X, Deng H. Highly efficient smoothing of Inconel 718 via electrochemical-based isotropic etching polishing. Precis Eng-J Int Soc Precis Eng Nanotechnol 2021;71:119–29. https://doi.org/10.1016/j.precisioneng.2021.03.005.
[3] Ando M, Negishi M, Takimoto M, Deguchi A, Nakamura N. Super-smooth polishing on aspherical surfaces.2. In: Achievement of a super-smooth polishing. International conference on optical fabrication and testing. 2576; 1995. p. 348–56 [Tokyo, Japan], https://doi.org/10.1117/12.215613.
[4] Bonora S, Pilar J, Lucianetti A, Mocek T. Design of deformable mirrors for high power lasers. High Power Laser Sci Eng 2016:4. https://doi.org/10.1017/hpl.2016.14.
[5] Carter RO. The effect of metal optical constants on far- and mid-infrared reflection—absorption. Spectroc Acta Pt A-Molec Biomolec Spectr 1991;47:551–61. https://doi.org/10.1016/0584-8539(91)80071-p.
[6] Cheng H, Dong Z, Ye X, Tam H-Y. Subsurface damages of fused silica developed during deterministic small tool polishing. Opt Express 2014;22:18588–603. https://doi.org/10.1364/oe.22.018588.
[7] de Rooij DMR. Electrochemical methods: fundamentals and applications. Anti-Corros Methods Mater 2003:50. https://doi.org/10.1108/acmm.2003.12850eae.001.
[8] Feigl T, Perske M, Pauer H, Fiedler T, Zeitner U, Leitel R, et al. Sub-aperture EUV collector with dual-wavelength spectral purity filter. In: Extreme ultraviolet (EUV) lithography VI conference. 9422; 2015. https://doi.org/10.1117/12.2175666 [p. DNS Electronics, LLC.San Jose, CA].
[9] Flitt HJ, Schweinsberg DP. Synthesis, matching and deconstruction of polarization curves for the active corrosion of zinc in aerated near-neutral NaCl solutions. Corros Sci. 2010;52:1905–14. https://doi.org/10.1016/j.corsci.2010.02.046.
[10] Han W, Fang F. Fundamental aspects and recent developments in electropolishing. Int J Mach Tool Manuf 2019;139:1–23. https://doi.org/10.1016/j.ijmachtools.2019.01.001.
[11] Jacquet PA. Electrolytic polishing of metallic surfaces. Met Finish 1949;47:48–54.
[12] Keong KG, Sha W, Malinov S. Hardness evolution of electroless nickel-phosphorus deposits with thermal processing. Surf Coat Technol 2003;168:263–74. https://doi.org/10.1016/s0257-8972(03)00209-3.
[13] Kim D, Son K, Sung D, Kim Y, Chung W. Effect of added ethanol in ethylene glycol-NaCl electrolyte on titanium electropolishing. Corros Sci 2015;98:494–9. https://doi.org/10.1016/j.corsci.2015.05.057.
[14] Koumvakalis N, Lee CS, Bass M. Intensity-dependent absorption in cu and ag metal mirrors - the role of temperature and surface roughness. IEEE J Quantum Electron 1983;19:1482–5. https://doi.org/10.1109/jqe.1983.1071739.
[15] Kwon GD, Kim YW, Moyen E, Keum DH, Lee YH, Baik S, et al. Controlled electropolishing of copper foils at elevated temperature. Appl Surf Sci 2014;307:731–5. https://doi.org/10.1016/j.apsusc.2014.04.144.
[16] Landolt D, Chauvy PF, Zinger O. Electrochemical micromachining, polishing and surface structuring of metals: fundamental aspects and new developments. Electrochim Acta 2003;48:3185–201. https://doi.org/10.1016/s0013-4686(03)00368-2.
[17] Li M, Huang Z, Dong T, Mao M, Lyu B, Yuan J. Surface integrity of bearing steel element with a new high-efficiency shear thickening polishing technique. In: 4th CIRP conference on surface integrity (CSI). 71; 2018. p. 313–6 [Tianjin, Peoples R China], https://doi.org/10.1016/j.procir.2018.05.030.
[18] Martyak NM. Characterization of thin electroless nickel coatings. Chem Mat 1994;6:1667–74. https://doi.org/10.1021/cm00046a019.
[19] Menapace JA, Ehrmann PR, Bickel RC. Magnetorheological finishing (MRF) of potassium dihydrogen phosphate (KDP) crystals: nonaqueous fluids development, optical finish, and laser damage performance at 1064 nm and 532 nm. In: Proceedings of the SPIE - the international society for optical engineering. 7504; 2009. https://doi.org/10.1117/12.836913 [P.750414 (750412 pp.)-750414 (750412 pp.).Boulder, CO, USA].
[20] Mojarad N, Gobrecht J, Ekinci Y. Interference lithography at EUV and soft X-ray wavelengths: principles, methods, and applications. Microelectron Eng 2015;143:55–63. https://doi.org/10.1016/j.mee.2015.03.047.
[21] Namba Y, Shimomura T, Fushiki A, Beaucamp A, Inasaki I, Kunieda H, et al. Ultra-precision polishing of electroless nickel molding dies for shorter wavelength applications. CIRP Ann-Manuf Technol 2008;57:337–40. https://doi.org/10.1016/j.cirp.2008.03.077.
[22] Oseki S, Oyabu S, Ishihara D, Enya K, Haze K, Kotani T, et al. Coronagraphic demonstration experiment using aluminum mirrors for space infrared astronomical observations. Publ Astron Soc Pac 2015;127:1077–83. https://doi.org/10.1086/683397.
[23] Reggiani RC, Mazza F, Sivieri E. Electrochemical polishing of titanium in perchloric-methanolic solutions. Mater Chem Phys 1979;4:149–58.
[24] Risse S, Gebhardt A, Steinkopf R, Giggel V. NiP plated mirrors for astronomy and space. In: 7th international conference European Society for Precision Engineering and Nanotechnology, EUSPEN 2007. 2; 2007. p. 348–51 [Bremen, Germany].
[25] Risse S, Gebhardt A, Kolbmuller A, Steinkopf R, Schurmann M, Jobst J, et al. Ultra-precise optical mirrors with thick amorphous silicon layer. In: 11th international conference of the European Society for Precision Engineering and Nanotechnology. 2. Italy: Como; 2011. p. 337–40. https://doi.org/10.1364/OIC.2010.PDWD15.
[26] Rohloff R-R, Gebhardt A, Schönherr V, Risse S, Kinast J, Scheiding S, et al. A novel athermal approach for high-performance cryogenic metal optics. In: Modern technologies in space-and ground-based telescopes and instrumentation. 7739; 2010. p. 1526–39 [San Diego, CA], https://doi.org/10.1117/12.856983.

[27] Rymell L, Malmqvist L, Berglund M, Hertz HM. Liquid-jet target laser-plasma sources for EUV and X-ray lithography. Microelectron Eng 1999;46:453–5. https://doi.org/10.1016/s0167-9317(99)00036-2.
[28] Saedi M, Sfiligoj C, Verhoeven J, Frenken JWM. Effect of rubidium incorporation on the optical properties and intermixing in Mo/Si multilayer mirrors for EUV lithography applications. Appl Surf Sci 2020:507. https://doi.org/10.1016/j.apsusc.2019.144951.
[29] Segers M, Bougeard M, Caprin E, Ceccotti T, Normand D, Schmidt M, et al. Development of a laser-produced plasma source at 13.5 nm for the French extreme ultraviolet lithography test bench. Microelectron Eng 2002;61-2:139–44. https://doi.org/10.1016/s0167-9317(02)00578-6.
[30] Sepulveda M, Quintero D, Castano JG, Echeverria F. Improved two-step Brytal process for electropolishing of aluminum alloys. Corros Sci 2018;136:386–92. https://doi.org/10.1016/j.corsci.2018.03.031.
[31] Steinkopf R, Gebhardt A, Scheiding S, Rohde M, Stenzel O, Gliech S, et al. Metal mirrors with excellent figure and roughness. Conference on optical fabrication, testing, and metrology III7102; 2008. p. 317–47 [Glasgow, SCOTLAND}, https://doi.org/10.1117/12.797702.
[32] Suzuki N, Hashimoto Y, Yasuda H, Yamaki S, Mochizuki Y. Prediction of polishing pressure distribution in CMP process with airbag type wafer carrier. CIRP Ann-Manuf Technol 2017;66:329–32. https://doi.org/10.1016/j.cirp.2017.04.088.
[33] Swapna MS, Nampoori VPN, Sankararaman S. Photoacoustics: a nondestructive evaluation technique for thermal and optical characterisation of metal mirrors. J Opt-India 2018;47:405–11. https://doi.org/10.1007/s12596-018-0471-0.
[34] Trost M, Schroeder S, Duparre A, Risse S, Feigl T, Zeitner UD, et al. Structured Mo/Si multilayers for IR-suppression in laser-produced EUV light sources. Opt Express 2013;21:27852–64. https://doi.org/10.1364/oe.21.027852.
[35] Tsai FC, Yan BH, Kuan CY, Huang FY. A Taguchi and experimental investigation into the optimal processing conditions for the abrasive jet polishing of SKD61 mold steel. Int J Mach Tool Manuf 2008;48:932–45. https://doi.org/10.1016/j.ijmachtools.2007.08.019.
[36] Wang F, Zhang X, Deng H. A comprehensive study on electrochemical polishing of tungsten. Appl Surf Sci 2019;475:587–97. https://doi.org/10.1016/j.apsusc.2019.01.020.
[37] Wang H, Moriconi S, Sawhney K. Nano-precision metrology of X-ray mirrors with laser speckle angular measurement. Light-Sci Appl 2021:10. https://doi.org/10.1038/s41377-021-00632-4.
[38] Yang G, Wang B, Tawfiq K, Wei H, Zhou S, Chen G. Electropolishing of surfaces: theory and applications. Surf Eng 2017;33:149–66. https://doi.org/10.1080/02670844.2016.1198452.
[39] Yi R, Zhang Y, Zhang X, Fang F, Deng H. A generic approach of polishing metals via isotropic electrochemical etching. Int J Mach Tool Manuf 2020:150. https://doi.org/10.1016/j.ijmachtools.2020.103517.
[40] Yi R, Ji J, Zhan Z, Deng H. Mechanism study of electropolishing from the perspective of etching isotropy. J Mater Process Technol 2022:305. https://doi.org/10.1016/j.jmatprotec.2022.117599.
[41] Zhang SJ, To S, Wang SJ, Zhu ZW. A review of surface roughness generation in ultra-precision machining. Int J Mach Tool Manuf 2015;91:76–95. https://doi.org/10.1016/j.ijmachtools.2015.02.001.